Resolution of prestack depth migration

Luděk Klimeš
Department of Geophysics, Faculty of Mathematics and Physics, Charles University, Ke Karlovu 3, 121 16 Praha 2, Czech Republic, http://sw3d.cz/staff/klimes.htm

Summary

Explicit approximate equations describing the physical meaning of the migrated sections are derived. The equations are applicable to 3–D elastic migrations in 3–D isotropic or anisotropic, heterogeneous velocity models. The imaged combination of elastic parameters (reflectivity) depends on the selection of the polarizations of the incident and back–propagated wavefields and on the directions of propagation. The migrated section is then approximately equal to the convolution of the unknown exact reflectivity function with the local resolution function. The local resolution function depends on the aperture and on the imaging function. The imaging function is determined by the source time function and by the form of the imaging functional.

Keywords

Elastic waves, velocity model, seismic migration, resolution, wavefield inversion, seismic anisotropy.

1. Introduction

A general formulation of *prestack depth migration* based on imaging (mapping) incident and scattered wavefields, extrapolated into the velocity model by arbitrary numerical methods (Claerbout, 1971) is considered in this paper. A *common–shot* prestack depth migration is assumed since it is the most natural configuration from the physics point of view, although the same approach could simply be applied to other configurations. The presented theory is developed for *3–D elastic migrations* in 3–D isotropic or anisotropic, heterogeneous velocity models. Neither scalar acoustic wavefields nor 2-D migrations are investigated separately.

The purpose of this paper is to study the physical meaning and spatial resolution of the migrated images. Our resolution study is considerably more general than the resolution analyses performed by Wu & Toksöz (1987), Lecomte & Gelius (1998) and Lecomte (1999) for the scalar wave equation in acoustic media.

Although the migrations are mostly performed in the isotropic velocity models, we shall present the equations in a general form suitable for elastic waves in heterogeneous anisotropic velocity models, because the assumption of isotropic velocity models or of isotropic perturbations provide for no considerable simplification of the theory. The equations expressed in terms of the general stiffness matrix c_{ijkl} are usually more concise and clear than the analogous explicit isotropic equations.

We use both vectorial and componental notation. For example, either $\mathbf{x}$ or x_i may stand for three spatial coordinates x_1, x_2, x_3. The Einstein summation over repetitive lower–case Roman subscripts corresponding to the 3 spatial coordinates is used throughout the paper.

In: Seismic Waves in Complex 3–D Structures, Report 21 (Department of Geophysics, Charles University, Prague, 2011), pp. 27–45

2. Velocity model and the elastodynamic equation

The velocity model of the geological structure is described in terms of the material parameters

$$\varrho = \varrho(\mathbf{x}) \ , \quad c_{ijkl} = c_{ijkl}(\mathbf{x}) \quad , \tag{1}$$

where $\mathbf{x} = (x_1, x_2, x_3)$ are spatial coordinates. We assume that velocity model $\varrho(\mathbf{x})$ and $c_{ijkl}(\mathbf{x})$ is smooth.

The geological structure is described in terms of the unknown material parameters

$$\varrho(\mathbf{x}) + \delta\varrho(\mathbf{x}) \ , \quad c_{ijkl}(\mathbf{x}) + \delta c_{ijkl}(\mathbf{x}) \quad , \tag{2}$$

where $\delta\varrho(\mathbf{x})$ and $\delta c_{ijkl}(\mathbf{x})$ represent the differences between the geological structure and the velocity model. Differences $\delta\varrho(\mathbf{x})$ and $\delta c_{ijkl}(\mathbf{x})$ are assumed to be small, but their dependence on coordinates $\mathbf{x}$ may be rough.

Seismic wavefield $u_i(\mathbf{x}, t)$ in the velocity model is subject to the elastodynamic equation

$$\varrho(\mathbf{x}) \ \ddot{u}_i(\mathbf{x}, t) = [c_{ijkl}(\mathbf{x}) \ u_{k,l}(\mathbf{x}, t)]_{,j} + f_i(\mathbf{x}, t) \tag{3}$$

for displacement $u_i(\mathbf{x}, t)$, where the dot $\dot{}$ stands for the derivative with respect to time t, and subscript $_{,j}$ following a comma stands for the partial derivative with respect to Cartesian spatial coordinate x_j. Term $f_i(\mathbf{x}, t)$ represents the source of the wavefield.

First–order perturbation (variation) δ of elastodynamic equation (3) yields the elastodynamic equation

$$\varrho(\mathbf{x}) \ \ddot{\delta u}_i(\mathbf{x}, t) = [c_{ijkl}(\mathbf{x}) \ \delta u_{k,l}(\mathbf{x}, t)]_{,j} - \delta\varrho(\mathbf{x}) \ \ddot{u}_i(\mathbf{x}, t) + [\delta c_{ijkl}(\mathbf{x}) \ u_{k,l}(\mathbf{x}, t)]_{,j} \tag{4}$$

for the first–order wavefield perturbation $\delta u_i(\mathbf{x}, t)$ due to medium perturbations $\delta c_{ijkl}(\mathbf{x})$ and $\delta\varrho(\mathbf{x})$. We shall refer to $\delta u_i(\mathbf{x}, t)$ as the *scattered wavefield*.

Elastodynamic Green tensor $G_{km}(\mathbf{x}, \mathbf{x}', t)$, corresponding to elastodynamic equation (1) in the velocity model, is defined by equation (Červený, 2001, eq. 2.5.37)

$$\varrho(\mathbf{x}) \ \ddot{G}_{im}(\mathbf{x}, \mathbf{x}', t-t') = [c_{ijkl}(\mathbf{x}) \ G_{km,l}(\mathbf{x}, \mathbf{x}', t-t')]_{,j} + \delta_{im} \, \delta(\mathbf{x} - \mathbf{x}') \, \delta(t-t') \tag{5}$$

with the zero initial conditions for $t-t' \leq 0$. The spatial partial derivatives in elastodynamic equation (5) are related to coordinates x_i. Here $\delta(\mathbf{x})$ and $\delta(t)$ are the 3–D and 1–D Dirac distributions.

In this paper, we shall mostly work in the frequency domain with 1–D Fourier transform

$$\widehat{u}_i(\mathbf{x}, \omega) = \widehat{\delta}(\omega) \int \mathrm{d}t \ u_i(\mathbf{x}, t) \ \exp(\mathrm{i}\omega t) \tag{6}$$

of the displacement, and with the analogous Fourier transform of the elastodynamic Green tensor. Here $\widehat{\delta}(\omega)$ is a constant equal to the 1–D Fourier transform of the 1–D Dirac distribution $\delta(t)$.

3. Migration

In our approach, prestack depth migration may be decomposed into the following steps (Claerbout, 1971): (a) *extrapolation* of the wavefields from the source and receiver points into the velocity model, (b) *decomposition* of the extrapolated wavefields into waves of different properties, (c) *imaging* the extrapolated and decomposed wavefields.

3.1. Extrapolation

Assume that seismic wavefield $u_i(\mathbf{x}'',t)+\delta u_i(\mathbf{x}'',t)$ is recorded at the receivers covering the *receiver area* along the Earth surface with a sufficient density to allow for the back propagation of scattered wavefield $\delta u_i(\mathbf{x}'',t)$ into the velocity model. Scattered wavefield $\delta u_i(\mathbf{x}'',t)$ is approximated by the solution of elastodynamic equation (4) for the first–order wavefield perturbation.

Let us denote by $U_i(\mathbf{x},t)$ the scattered wavefield $\delta u_i(\mathbf{x}'',t)$ back–propagated from the receiver area into the velocity model. Note that we do not back–propagate the complete scattered wavefield but only its part recorded in the receiver area. Moreover, the recorded wavefield may also be reduced by application of the aperture weighting factor $a(\mathbf{x}'')$ dependent on the receiver positions $\mathbf{x}''$.

In the time domain, we can back–propagate the scattered wavefield by taking the scattered wavefield at the receivers with opposite time, propagating it into the target zone using the representation theorem, and then changing the sign of time again. The opposite time in the time domain corresponds to the complex–conjugate wavefield in the frequency domain. In the frequency domain, we thus take the complex–conjugate scattered wavefield at the receivers, insert it together with the Green tensor into the representation theorem, and complex–conjugate the result.

In the frequency domain, the forward propagation from point $\mathbf{x}'$ situated in the vicinity of point $\mathbf{x}$ to point $\mathbf{x}''$ situated on the surface covered by the receivers is described by Green tensor $\widehat{G}_{im}(\mathbf{x}'',\mathbf{x}',\omega)$. The back propagation from point $\mathbf{x}''$ to point $\mathbf{x}$ is then described by complex–conjugate Green tensor $\widehat{G}^*_{in}(\mathbf{x},\mathbf{x}'',\omega)=\widehat{G}^*_{ni}(\mathbf{x}'',\mathbf{x},\omega)$.

The scattered wavefield can be back–propagated from surface S to point $\mathbf{x}$ using the frequency–domain representation theorem (Červený, 2001, eq. 2.6.4):

$$\widehat{U}_i(\mathbf{x},\omega)=\frac{1}{\widehat{\delta}(\omega)}\int_S \mathrm{d}S(\mathbf{x}'')\,a(\mathbf{x}'')\,\big[\widehat{G}^*_{ni}(\mathbf{x}'',\mathbf{x},\omega)\,n_j(\mathbf{x}'')\,c_{njkl}(\mathbf{x}'')\,\widehat{\delta u}_{k,l}(\mathbf{x}'',\omega) - \widehat{G}^*_{ni,j}(\mathbf{x}'',\mathbf{x},\omega)\,c_{njkl}(\mathbf{x}'')\,\widehat{\delta u}_k(\mathbf{x}'',\omega)\,n_l(\mathbf{x}'')\big] \quad , \qquad (7)$$

where $\widehat{\delta}(\omega)$ is a constant equal to the 1–D Fourier transform of the 1–D Dirac distribution $\delta(t)$. Note that Červený (2001) chose $\widehat{\delta}(\omega)=1$. Unit normal $n_j(\mathbf{x}'')$ to surface S is pointing in accord with the forward propagation of the incident wavefield. The partial derivatives in (7) are related to variable $\mathbf{x}''$. The weighting factor of $a(\mathbf{x}'')$ is inserted to account for possible windowing of the seismic records (time sections) at receiver points $\mathbf{x}''$. If we do not need windowing of the seismic records, we may put $a(\mathbf{x}'')=1$.

The approximate incident wavefield $u_i(\mathbf{x},t)$ and the back–propagated scattered wavefield $U_i(\mathbf{x},t)$ may be calculated in velocity model $\varrho(\mathbf{x})$, $c_{ijkl}(\mathbf{x})$ by any convenient numerical method.

3.2. Decomposition

To resolve more than a single linear combination of medium perturbations $\delta\varrho(\mathbf{x})$ and $\delta c_{ijkl}(\mathbf{x})$, it is desirable to attempt to decompose both the approximate incident wavefield $u_i(\mathbf{x},t)$ and the back–propagated scattered wavefield $U_i(\mathbf{x},t)$ at each point $\mathbf{x}$ locally into P and S waves or, better, into P waves and two polarizations of S waves. Such a decomposition may conveniently be accomplished by a proper choice of imaging functionals.

In addition, if the waves incident from considerably different directions can locally be distinguished in the approximate incident wavefield $u_i(\mathbf{x},t)$ or back–propagated scattered wavefield $U_i(\mathbf{x},t)$, the respective wavefield may be decomposed into the parts corresponding to the different propagation directions, particularly for the purposes of the "amplitude–versus–angle" analysis.

If the decomposition into the parts corresponding to the different propagation directions is not possible, the amplitude–versus–angle analysis may be facilitated by splitting the receiver area into two or more smaller receiver areas, e.g., by applying the aperture weighting factor $a(\mathbf{x}'')$ dependent on receiver positions $\mathbf{x}''$. This splitting, however, deteriorates the lateral spatial resolution of the migrated sections.

If any of the above decompositions is applicable, let $u_i(\mathbf{x},t)$ denote hereinafter one selected part of the decomposed approximate incident wavefield and $U_i(\mathbf{x},t)$ one selected part of the back–propagated scattered wavefield.

3.3. Imaging

We have, at each point $\mathbf{x}$, time functions $u_i(\mathbf{x},t)$ and $U_i(\mathbf{x},t)$ representing selected parts of the incident wavefield and of the back–propagated scattered wavefield.

Assume that *imaging functional* (mapping procedure)

$$M(\bullet,\bullet): \quad u_i, U_i \longrightarrow m = M(u_i, U_i) \quad , \tag{8}$$

maps the pairs of functions $u_i = u_i(t')$ and $U_i = U_i(t)$ onto the real or complex numbers.

The *migrated section* is then

$$m(\mathbf{x}) = M\big(u_i(\mathbf{x},t'), U_i(\mathbf{x},t)\big) \quad . \tag{9}$$

We assume that the imaging functional (8) is linear with respect to the second argument representing the back–propagated scattered wavefield.

4. Born approximation of the back–propagated scattered wavefield

4.1. Born approximation of the scattered wavefield

The wavefield scattered by medium perturbations $\delta c_{ijkl}(\mathbf{x})$ and $\delta\varrho(\mathbf{x})$ can be approximated by the solution $\delta u(\mathbf{x}'',t)$ of elastodynamic equation (4). The Fourier transform $\widehat{\delta u}_i(\mathbf{x}'',\omega)$ of scattered wavefield $\delta u(\mathbf{x}'',t)$ can be expressed in the form of the first–order Born approximation (Červený, 2001, eq. 2.6.18)

$$\widehat{\delta u}_i(\mathbf{x}'',\omega) \approx \frac{1}{\widehat{\delta}(\omega)} \int \mathrm{d}\mathbf{x}' \, \big[- \widehat{G}_{im,j}(\mathbf{x}'',\mathbf{x}',\omega) \delta c_{mjkl}(\mathbf{x}') \widehat{u}_{k,l}(\mathbf{x}',\omega) - (\mathrm{i}\omega)^2 \widehat{G}_{im}(\mathbf{x}'',\mathbf{x}',\omega) \delta\varrho(\mathbf{x}') \widehat{u}_m(\mathbf{x}',\omega) \big] \quad , \tag{10}$$

where the partial derivatives are related to variable $\mathbf{x}'$. Here $\widehat{\delta}(\omega)$ is a constant equal to the 1–D Fourier transform of the 1–D Dirac distribution $\delta(t)$. Note that Červený (2001) chose $\widehat{\delta}(\omega) = 1$.

4.2. Decomposing the incident wave into arrivals and the Green tensor into elementary waves

We assume that incident wavefield $\widehat{u}_i(\mathbf{x}',\omega)$ in (10) is composed of several arrivals $\widehat{u}_m^{\mathrm{Arr}}(\mathbf{x}',\omega)$,

$$\widehat{u}_i(\mathbf{x}',\omega) = \sum_{\mathrm{Arr}} \widehat{u}_i^{\mathrm{Arr}}(\mathbf{x}',\omega) \quad . \tag{11}$$

Then also the scattered wavefield is composed of several arrivals.

The ray–theory approximation of the Green tensor is composed of the elementary Green tensors corresponding to the individual elementary waves:

$$\widehat{G}_{im}(\mathbf{x}'',\mathbf{x},\omega) = \sum_{\mathrm{EW}} \widehat{G}_{im}^{\mathrm{EW}}(\mathbf{x}'',\mathbf{x},\omega) \quad . \tag{12}$$

The corresponding prestack depth migrated section is then composed of the migrated sections corresponding to all combinations of the above mentioned arrivals and elementary waves:

$$\widehat{m}(\mathbf{x}) = \sum_{\mathrm{Arr}} \sum_{\mathrm{EW}} \widehat{m}^{\mathrm{ArrEW}}(\mathbf{x}) \quad . \tag{13}$$

In the following, we shall consider just one of the arrivals and one of the elementary waves, but omit superscripts $^{\mathrm{Arr}}$ and $^{\mathrm{EW}}$ for the sake of conciseness and simplicity.

In the following, we shall also assume that each arrival of the incident wave can be expressed in terms of unit polarization vector $E_k(\mathbf{x}')$ and local spectrum $\widehat{f}(\mathbf{x}',\omega)$:

$$\widehat{u}_k^{\mathrm{Arr}}(\mathbf{x}',\omega) = E_k(\mathbf{x}') \, \widehat{f}(\mathbf{x}',\omega) \quad . \tag{14}$$

4.3. Ray–theory approximation of the Green tensor

We shall now apply the ray–theory approximation of the Green tensor. We parametrize the rays from point $\mathbf{x}$ to point $\mathbf{x}''$ by the initial slowness vectors at point $\mathbf{x}$. The rays corresponding to the small area $\mathrm{d}S_p(\mathbf{x})$ situated on the slowness surface then create a narrow ray tube. We denote by $\mathrm{d}S_\perp(\mathbf{x}'')$ the area of the perpendicular cross–section

of this ray tube at point $\mathbf{x}''$. The relative geometrical spreading of Červený (2001, eq. 4.10.11) then reads

$$L(\mathbf{x}'',\mathbf{x}) = \sqrt{\frac{v(\mathbf{x}'')v(\mathbf{x})\,\mathrm{d}S_\perp(\mathbf{x}'')}{c(\mathbf{x}'')c(\mathbf{x})\,\mathrm{d}S_p(\mathbf{x})}} \quad , \tag{15}$$

where c is the phase velocity and v is the ray velocity, both corresponding to the ray leading from point $\mathbf{x}$ to point $\mathbf{x}''$.

Note that the slowness surface at point $\mathbf{x}$ may be parametrized by coordinates $\boldsymbol{\gamma} = (\gamma_1, \gamma_2)$ along the unit sphere composed of the normalized initial slowness vectors $\mathbf{p}(\mathbf{x})/|\mathbf{p}(\mathbf{x})|$. Then $\mathbf{p}(\mathbf{x}) = \mathbf{p}(\mathbf{x},\boldsymbol{\gamma})$. The small area $\mathrm{d}S_p(\mathbf{x})$ situated on the slowness surface corresponding to small area $\mathrm{d}\Gamma$ situated on the unit sphere is determined by relation

$$\frac{\mathrm{d}S_p(\mathbf{x})}{\mathrm{d}\Gamma} = \frac{v(\mathbf{x},\boldsymbol{\gamma})}{[c(\mathbf{x},\boldsymbol{\gamma})]^3} \quad . \tag{16}$$

The ray–theory approximation of the elementary Green tensor corresponding to a particular elementary wave reads (Červený, 2001, eq. 5.4.24):

$$\widehat{G}_{im}(\mathbf{x}'',\mathbf{x},\omega) \approx \widehat{\delta}(\omega)\frac{e_i(\mathbf{x}'',\boldsymbol{\gamma})e_m(\mathbf{x},\boldsymbol{\gamma})T(\mathbf{x}'',\mathbf{x})}{4\pi L(\mathbf{x}'',\mathbf{x})\sqrt{\varrho(\mathbf{x}'')c(\mathbf{x}'',\boldsymbol{\gamma})\varrho(\mathbf{x})c(\mathbf{x},\boldsymbol{\gamma})}}\ \exp[\mathrm{i}\omega\tau(\mathbf{x}'',\mathbf{x})] \quad , \tag{17}$$

where e_K are the polarization vectors and c is the phase velocity. Here $T(\mathbf{x}'',\mathbf{x})$ is the accumulated reciprocal transmission coefficient describing the amplitude losses between points $\mathbf{x}$ and $\mathbf{x}''$ due to attenuation and due to reflections and scattering into directions leading outside the vicinity of point $\mathbf{x}''$. In an ideal case, $T(\mathbf{x}'',\mathbf{x}) \approx 1$. Possible phase shifts due to caustics are also included in $T(\mathbf{x}'',\mathbf{x})$, but are annulled by the combination of forward propagation and back propagation. For $\omega < 0$, $T(\mathbf{x}'',\mathbf{x})$ is complex–conjugate, but this complex–conjugacy is compensated by the combination of forward propagation and back propagation.

Since points $\mathbf{x}$ and $\mathbf{x}'$ are close, quantities $\boldsymbol{\gamma}$, $e_i(\mathbf{x}'',\boldsymbol{\gamma})$, $e_m(\mathbf{x},\boldsymbol{\gamma})$, $T(\mathbf{x}'',\mathbf{x})$, $L(\mathbf{x}'',\mathbf{x})$, $c(\mathbf{x}'',\boldsymbol{\gamma})$, $c(\mathbf{x},\boldsymbol{\gamma})$ corresponding to the ray from $\mathbf{x}$ to $\mathbf{x}''$, and quantities $\boldsymbol{\gamma}'$, $e_i(\mathbf{x}'',\boldsymbol{\gamma}')$, $e_m(\mathbf{x}',\boldsymbol{\gamma}')$, $T(\mathbf{x}'',\mathbf{x}')$, $L(\mathbf{x}'',\mathbf{x}')$, $c(\mathbf{x}'',\boldsymbol{\gamma}')$, $c(\mathbf{x}',\boldsymbol{\gamma}')$ corresponding to the ray from $\mathbf{x}'$ to $\mathbf{x}''$, are approximately equal. On the other hand, the difference between two–point travel times $\tau(\mathbf{x}'',\mathbf{x})$ and $\tau(\mathbf{x}'',\mathbf{x}')$ is essential for our study.

We apply the high–frequency approximation of the spatial derivatives of the Green tensor and of the incident wavefield:

$$\frac{\partial\widehat{G}_{im}}{\partial x_j''}(\mathbf{x}'',\mathbf{x},\omega) \approx \mathrm{i}\omega p_j(\mathbf{x}'',\boldsymbol{\gamma})\,\widehat{G}_{im}(\mathbf{x}'',\mathbf{x},\omega) \quad , \tag{18}$$

$$\frac{\partial\widehat{G}_{im}}{\partial x_j'}(\mathbf{x}'',\mathbf{x}',\omega) \approx -\mathrm{i}\omega p_j(\mathbf{x}',\boldsymbol{\gamma}')\,\widehat{G}_{im}(\mathbf{x}'',\mathbf{x}',\omega) \quad , \tag{19}$$

$$\widehat{u}_{k,l}(\mathbf{x}',\omega) \approx \mathrm{i}\omega P_l(\mathbf{x}')\,\widehat{u}_k(\mathbf{x}',\omega) \quad . \tag{20}$$

Angular coordinates $\boldsymbol{\gamma}$ correspond to the ray leading from point $\mathbf{x}$ to point $\mathbf{x}''$, whereas angular coordinates $\boldsymbol{\gamma}'$ correspond to the ray leading from point $\mathbf{x}'$ to point $\mathbf{x}''$. Since points $\mathbf{x}$ and $\mathbf{x}'$ are close, $\boldsymbol{\gamma}' \approx \boldsymbol{\gamma}$.

We insert approximations (19) and (20) into Born approximation (10):

$$\widehat{\delta u}_i(\mathbf{x}'',\omega) \approx \frac{(\mathrm{i}\omega)^2}{\widehat{\delta}(\omega)}\int \mathrm{d}\mathbf{x}'\ \widehat{G}_{im}(\mathbf{x}'',\mathbf{x}',\omega)\big[\delta c_{mjkl}(\mathbf{x}')p_j(\mathbf{x}',\boldsymbol{\gamma}')\widehat{u}_k(\mathbf{x}',\omega)P_l(\mathbf{x}') - \delta\varrho(\mathbf{x}')\widehat{u}_m(\mathbf{x}',\omega)\big] \quad . \tag{21}$$

4.4. Back–propagating scattered wavefield

We insert approximation (21) of the scattered wavefield into back propagation (7) and obtain

$$\widehat{U}_i(\mathbf{x},\omega) \approx \frac{(\mathrm{i}\omega)^2}{\widehat{\delta}(\omega)} \int \mathrm{d}\mathbf{x}' \; \widehat{D}_{im}(\mathbf{x},\mathbf{x}',\omega) \big[\delta c_{mjkl}(\mathbf{x}') p_j(\mathbf{x}',\boldsymbol{\gamma}') \widehat{u}_k(\mathbf{x}',\omega) P_l(\mathbf{x}') - \delta\varrho(\mathbf{x}') \widehat{u}_m(\mathbf{x}',\omega)\big] \quad , \tag{22}$$

where

$$\widehat{D}_{im}(\mathbf{x},\mathbf{x}',\omega) = \frac{1}{\widehat{\delta}(\omega)} \int_S \mathrm{d}S(\mathbf{x}'')\, a(\mathbf{x}'') \left[\widehat{G}^*_{ni}(\mathbf{x}'',\mathbf{x},\omega)\, n_j(\mathbf{x}'')\, c_{njkl}(\mathbf{x}'')\, \widehat{G}_{km,l}(\mathbf{x}'',\mathbf{x}',\omega) - \widehat{G}^*_{ni,j}(\mathbf{x}'',\mathbf{x},\omega)\, c_{njkl}(\mathbf{x}'')\, \widehat{G}_{km}(\mathbf{x}'',\mathbf{x}',\omega)\, n_l(\mathbf{x}'')\right] \tag{23}$$

is the Green tensor from point $\mathbf{x}'$, back–propagated from the receiver array to point $\mathbf{x}$ situated close to point $\mathbf{x}'$. The partial derivatives in (23) are related to variable $\mathbf{x}''$.

We insert high–frequency approximation (18) into (23) and obtain

$$\widehat{D}_{im}(\mathbf{x},\mathbf{x}',\omega) \approx \frac{\mathrm{i}\omega}{\widehat{\delta}(\omega)} \int_S \mathrm{d}S(\mathbf{x}'')\, a(\mathbf{x}'')\, \widehat{G}^*_{ni}(\mathbf{x}'',\mathbf{x},\omega)\, \widehat{G}_{km}(\mathbf{x}'',\mathbf{x}',\omega) \times \big[n_j(\mathbf{x}'')\, c_{njkl}(\mathbf{x}'')\, p_l(\mathbf{x}'',\boldsymbol{\gamma}) + p_j(\mathbf{x}'',\boldsymbol{\gamma})\, c_{njkl}(\mathbf{x}'')\, n_l(\mathbf{x}'')\big] \,. \tag{24}$$

We insert ray–theory approximation (17) for both the Green tensors, apply approximation

$$e_k(\mathbf{x}'',\boldsymbol{\gamma}') \approx e_k(\mathbf{x}'',\boldsymbol{\gamma}) \quad , \tag{25}$$

and use identity

$$c_{njkl}(\mathbf{x}'') e_n(\mathbf{x}'',\boldsymbol{\gamma}) e_k(\mathbf{x}'',\boldsymbol{\gamma}) p_l(\mathbf{x}'',\boldsymbol{\gamma}) = \varrho(\mathbf{x}'')\, v_j(\mathbf{x}'',\boldsymbol{\gamma}) \quad , \tag{26}$$

where v_j is the ray–velocity vector. Equation (24) then reads

$$\widehat{D}_{im}(\mathbf{x},\mathbf{x}',\omega) \approx \mathrm{i}\omega\widehat{\delta}(\omega) \int_S \mathrm{d}S(\mathbf{x}'')\, a(\mathbf{x}'') \times \frac{2\, n_j(\mathbf{x}'')\, v_j(\mathbf{x}'',\boldsymbol{\gamma})\, e_i(\mathbf{x},\boldsymbol{\gamma}) e_m(\mathbf{x}',\boldsymbol{\gamma}') T^*(\mathbf{x}'',\mathbf{x}) T(\mathbf{x}'',\mathbf{x}')}{16\pi^2 L(\mathbf{x}'',\mathbf{x}) L(\mathbf{x}'',\mathbf{x}') \sqrt{c(\mathbf{x}'',\boldsymbol{\gamma})\varrho(\mathbf{x}) c(\mathbf{x},\boldsymbol{\gamma}) c(\mathbf{x}'',\boldsymbol{\gamma}')\varrho(\mathbf{x}') c(\mathbf{x}',\boldsymbol{\gamma}')}} \times \exp\{\mathrm{i}\omega[\tau(\mathbf{x}'',\mathbf{x}') - \tau(\mathbf{x}'',\mathbf{x})]\} \quad . \tag{27}$$

We now apply approximations

$$\begin{aligned} T(\mathbf{x}'',\mathbf{x}') &\approx T(\mathbf{x}'',\mathbf{x}) \quad , \\ L(\mathbf{x}'',\mathbf{x}') &\approx L(\mathbf{x}'',\mathbf{x}) \quad , \\ c(\mathbf{x}'',\boldsymbol{\gamma}') &\approx c(\mathbf{x}'',\boldsymbol{\gamma}) \quad , \\ c(\mathbf{x}',\boldsymbol{\gamma}') &\approx c(\mathbf{x},\boldsymbol{\gamma}) \quad , \\ \rho(\mathbf{x}) &\approx \rho(\mathbf{x}') \quad , \end{aligned} \tag{28}$$

and obtain

$$\widehat{D}_{im}(\mathbf{x},\mathbf{x}',\omega) \approx \frac{\mathrm{i}\omega\widehat{\delta}(\omega)}{8\pi^2} \int_S \mathrm{d}S(\mathbf{x}'')\, a(\mathbf{x}'')\, \frac{n_j(\mathbf{x}'')\, v_j(\mathbf{x}'',\boldsymbol{\gamma})\, e_i(\mathbf{x},\boldsymbol{\gamma}) e_m(\mathbf{x}',\boldsymbol{\gamma}') |T(\mathbf{x}'',\mathbf{x})|^2}{[L(\mathbf{x}'',\mathbf{x})]^2 c(\mathbf{x}'',\boldsymbol{\gamma})\varrho(\mathbf{x}') c(\mathbf{x},\boldsymbol{\gamma})} \times \exp\{\mathrm{i}\omega[\tau(\mathbf{x}'',\mathbf{x}') - \tau(\mathbf{x}'',\mathbf{x})]\} \quad . \tag{29}$$

We insert relation (15) and relation

$$n_j(\mathbf{x}'')\, v_j(\mathbf{x}'',\boldsymbol{\gamma}) = \frac{\mathrm{d}S_\perp(\mathbf{x}'')}{\mathrm{d}S(\mathbf{x}'')}\, v(\mathbf{x}'',\boldsymbol{\gamma}) \tag{30}$$

between the area $\mathrm{d}S_\perp(\mathbf{x}'')$ of the perpendicular cross–section of a narrow ray tube and the area $\mathrm{d}S(\mathbf{x}'')$ of the cross–section of the narrow ray tube with the surface S of integration:

$$\widehat{D}_{im}(\mathbf{x},\mathbf{x}',\omega) \approx \frac{\mathrm{i}\omega\widehat{\delta}(\omega)}{8\pi^2}\int_S \mathrm{d}S(\mathbf{x}'')\, a(\mathbf{x}'')\, \frac{\mathrm{d}S_p(\mathbf{x})}{\mathrm{d}S(\mathbf{x}'')}\, \frac{e_i(\mathbf{x},\boldsymbol{\gamma})e_m(\mathbf{x}',\boldsymbol{\gamma}')|T(\mathbf{x}'',\mathbf{x})|^2}{v(\mathbf{x},\boldsymbol{\gamma})\varrho(\mathbf{x}')} \times \exp\{\mathrm{i}\omega[\tau(\mathbf{x}'',\mathbf{x}') - \tau(\mathbf{x}'',\mathbf{x})]\} \quad . \tag{31}$$

We apply relation (16) and the first–order paraxial approximation

$$\tau(\mathbf{x}'',\mathbf{x}') - \tau(\mathbf{x}'',\mathbf{x}) \approx -p_k(\mathbf{x},\boldsymbol{\gamma})\,(x'_k - x_k) \tag{32}$$

of the travel time at point $\mathbf{x}$, and obtain relation

$$\widehat{D}_{im}(\mathbf{x},\mathbf{x}',\omega) \approx \frac{\mathrm{i}\omega\widehat{\delta}(\omega)}{8\pi^2}\int_S \mathrm{d}S(\mathbf{x}'')\, a(\mathbf{x}'')\, \frac{\mathrm{d}\Gamma}{\mathrm{d}S(\mathbf{x}'')}\, \frac{e_i(\mathbf{x},\boldsymbol{\gamma})e_m(\mathbf{x}',\boldsymbol{\gamma}')|T(\mathbf{x}'',\mathbf{x})|^2}{[c(\mathbf{x},\boldsymbol{\gamma})]^3\varrho(\mathbf{x}')} \times \exp[\mathrm{i}\omega\, p_k(\mathbf{x},\boldsymbol{\gamma})\,(x_k - x'_k)] \quad . \tag{33}$$

The integrand is, except for the aperture weighting factor $a(\mathbf{x}'')$ and the reciprocal transmission coefficient $T(\mathbf{x}'',\mathbf{x})$ between target point $\mathbf{x}$ and receiver point $\mathbf{x}''$, independent of $\mathbf{x}''$.

We denote the angular domain (aperture) corresponding to all rays leading to the receiver area by Γ. The *aperture weighting function*

$$\begin{aligned} \boldsymbol{\gamma} \in \Gamma: &\quad A(\mathbf{x},\boldsymbol{\gamma}) = a(\mathbf{x}'')\, [T(\mathbf{x}'',\mathbf{x})]^2 \\ \boldsymbol{\gamma} \notin \Gamma: &\quad A(\mathbf{x},\boldsymbol{\gamma}) = 0 \end{aligned} \tag{34}$$

accounts both for the aperture limitation to directions $\boldsymbol{\gamma} \in \Gamma$, for possible windowing $a(\mathbf{x}'')$ of the seismic records (time sections) at receiver points $\mathbf{x}''$, and for the two–way accumulated reciprocal transmission coefficient between target point $\mathbf{x}'$ and receiver point $\mathbf{x}''$.

Integration over surface S in (33) may thus be extended to the whole solid angle (all directions):

$$\widehat{D}_{im}(\mathbf{x},\mathbf{x}',\omega) \approx \frac{\mathrm{i}\omega\widehat{\delta}(\omega)}{8\pi^2}\oint \mathrm{d}\Gamma\, A(\mathbf{x},\boldsymbol{\gamma})\, \frac{e_i(\mathbf{x},\boldsymbol{\gamma})e_m(\mathbf{x}',\boldsymbol{\gamma}')}{[c(\mathbf{x},\boldsymbol{\gamma})]^3\varrho(\mathbf{x}')}\, \exp[\mathrm{i}\omega\, p_k(\mathbf{x},\boldsymbol{\gamma})\,(x_k - x'_k)] \quad . \tag{35}$$

The back–propagated scattered wavefield $\widehat{U}_i(\mathbf{x},\omega)$ may be obtained from relation (22) by means of inserting (35),

$$\begin{aligned} \widehat{U}_i(\mathbf{x},\omega) \approx \frac{(\mathrm{i}\omega)^3}{8\pi^2}\int \mathrm{d}\mathbf{x}' \oint \mathrm{d}\Gamma\, A(\mathbf{x},\boldsymbol{\gamma})\, \frac{e_i(\mathbf{x},\boldsymbol{\gamma})e_m(\mathbf{x}',\boldsymbol{\gamma}')}{[c(\mathbf{x},\boldsymbol{\gamma})]^3\varrho(\mathbf{x}')} \\ \times [\delta c_{mjkl}(\mathbf{x}')p_j(\mathbf{x}',\boldsymbol{\gamma}')\widehat{u}_k(\mathbf{x}',\omega)P_l(\mathbf{x}') - \delta\varrho(\mathbf{x}')\widehat{u}_m(\mathbf{x}',\omega)] \exp[\mathrm{i}\omega\, p_k(\mathbf{x},\boldsymbol{\gamma})\,(x_k - x'_k)] \quad . \end{aligned} \tag{36}$$

We insert assumption (14) into relation (36), and obtain

$$\begin{aligned} \widehat{U}_i(\mathbf{x},\omega) \approx \frac{(\mathrm{i}\omega)^3}{8\pi^2}\int \mathrm{d}\mathbf{x}' \oint \mathrm{d}\Gamma\, A(\mathbf{x},\boldsymbol{\gamma})\, \frac{e_i(\mathbf{x},\boldsymbol{\gamma})e_m(\mathbf{x}',\boldsymbol{\gamma}')}{[c(\mathbf{x},\boldsymbol{\gamma})]^3\varrho(\mathbf{x}')}\, \widehat{f}(\mathbf{x}',\omega) \\ \times [\delta c_{mjkl}(\mathbf{x}')p_j(\mathbf{x}',\boldsymbol{\gamma}')E_k(\mathbf{x}')P_l(\mathbf{x}') - \delta\varrho(\mathbf{x}')E_m(\mathbf{x}')] \exp[\mathrm{i}\omega\, p_k(\mathbf{x},\boldsymbol{\gamma})\,(x_k - x'_k)] \quad . \end{aligned} \tag{37}$$

We now define the *angle–dependent reflectivity function*

$$\boxed{r(\mathbf{x}',\boldsymbol{\gamma}') = \frac{\delta\varrho(\mathbf{x}')E_m(\mathbf{x}')e_m(\mathbf{x}',\boldsymbol{\gamma}') - \delta c_{ijkl}(\mathbf{x}')P_i(\mathbf{x}')E_j(\mathbf{x}')p_k(\mathbf{x}',\boldsymbol{\gamma}')e_l(\mathbf{x}',\boldsymbol{\gamma}')}{2\ \varrho(\mathbf{x}')} \quad , \quad (38)}$$

and relation (37) reads

$$\widehat{U}_i(\mathbf{x},\omega) \approx \frac{-(\mathrm{i}\omega)^3}{4\pi^2}\int \mathrm{d}\mathbf{x}' \oint \mathrm{d}\Gamma\ A(\mathbf{x},\boldsymbol{\gamma})\ \frac{e_i(\mathbf{x},\boldsymbol{\gamma})}{[c(\mathbf{x},\boldsymbol{\gamma})]^3}\ \widehat{f}(\mathbf{x}',\omega)\, r(\mathbf{x}',\boldsymbol{\gamma}')\ \exp[\mathrm{i}\omega\, p_k(\mathbf{x},\boldsymbol{\gamma})\,(x_k - x_k')] \ . \quad (39)$$

Since $\boldsymbol{\gamma}' \approx \boldsymbol{\gamma}$ because points $\mathbf{x}$ and $\mathbf{x}'$ are close, we apply approximation

$$r(\mathbf{x}',\boldsymbol{\gamma}') \approx r(\mathbf{x}',\boldsymbol{\gamma}) \quad . \quad (40)$$

We also apply the first–order paraxial expansion

$$\widehat{f}(\mathbf{x}',\omega) \approx \widehat{f}(\mathbf{x},\omega)\ \exp[\mathrm{i}\omega\, P_k(\mathbf{x})\,(x_k' - x_k)] \quad (41)$$

of the travel time of the incident wave from point $\mathbf{x}$ to point $\mathbf{x}'$. Relation (39) then reads

$$\widehat{U}_i(\mathbf{x},\omega) \approx \frac{-(\mathrm{i}\omega)^3}{4\pi^2}\int \mathrm{d}\mathbf{x}' \oint \mathrm{d}\Gamma\ A(\mathbf{x},\boldsymbol{\gamma})\ \frac{e_i(\mathbf{x},\boldsymbol{\gamma})}{[c(\mathbf{x},\boldsymbol{\gamma})]^3}\ \widehat{f}(\mathbf{x},\omega) \times r(\mathbf{x}',\boldsymbol{\gamma})\ \exp\left\{\mathrm{i}\omega\,[p_k(\mathbf{x},\boldsymbol{\gamma}) - P_k(\mathbf{x})]\,(x_k - x_k')\right\} \quad . \quad (42)$$

We define the 3–D Fourier transform of the angle–dependent reflectivity function by equation

$$\widehat{r}(\mathbf{k},\boldsymbol{\gamma}) = \widehat{\delta}(\mathbf{k}) \int \mathrm{d}\mathbf{x}'\ r(\mathbf{x}',\boldsymbol{\gamma})\ \exp(-\mathrm{i}\, k_k\, x_k') \quad , \quad (43)$$

where constant $\widehat{\delta}(\mathbf{k})$ represents the 3–D Fourier transform of the 3–D Dirac distribution $\delta(\mathbf{x})$. Relation (42) then reads

$$\widehat{U}_i(\mathbf{x},\omega) \approx \frac{-(\mathrm{i}\omega)^3 \widehat{f}(\mathbf{x},\omega)}{4\pi^2\, \widehat{\delta}(\mathbf{k})} \oint \mathrm{d}\Gamma\ A(\mathbf{x},\boldsymbol{\gamma}) \frac{e_i(\mathbf{x},\boldsymbol{\gamma})}{[c(\mathbf{x},\boldsymbol{\gamma})]^3} \times \widehat{r}\big(\omega[\mathbf{p}(\mathbf{x},\boldsymbol{\gamma}) - \mathbf{P}(\mathbf{x})],\boldsymbol{\gamma}\big)\ \exp\left\{\mathrm{i}\omega\,[p_k(\mathbf{x},\boldsymbol{\gamma}) - P_k(\mathbf{x})]\, x_k\right\} \quad . \quad (44)$$

We transform the back–propagated scattered wavefield into the time domain using inverse 1–D Fourier transform

$$U_i(\mathbf{x},t) = \frac{1}{2\pi\, \widehat{\delta}(\omega)} \int \mathrm{d}\omega\ \widehat{U}_i(\mathbf{x},\omega)\ \exp(-\mathrm{i}\omega t) \quad , \quad (45)$$

and obtain relation

$$U_i(\mathbf{x},t) \approx \int \mathrm{d}\omega\ \frac{-(\mathrm{i}\omega)^3 \exp(-\mathrm{i}\omega t) \widehat{f}(\mathbf{x},\omega)}{8\pi^3\, \widehat{\delta}(\omega)\ \widehat{\delta}(\mathbf{k})} \oint \mathrm{d}\Gamma\ A(\mathbf{x},\boldsymbol{\gamma})\ \frac{e_i(\mathbf{x},\boldsymbol{\gamma})}{[c(\mathbf{x},\boldsymbol{\gamma})]^3} \times \widehat{r}\big(\omega[\mathbf{p}(\mathbf{x},\boldsymbol{\gamma}) - \mathbf{P}(\mathbf{x})],\boldsymbol{\gamma}\big)\ \exp\left\{\mathrm{i}\omega\,[p_k(\mathbf{x},\boldsymbol{\gamma}) - P_k(\mathbf{x})]\, x_k\right\} \quad . \quad (46)$$

5. Analysis of the migrated section

We assume that imaging functional (8) is linear with respect to the second argument representing the back–propagated scattered wavefield. This is our only assumption about the imaging functional.

5.1. Imaging function

The polarization of the scattered wavefield back–propagated from the direction given by $\boldsymbol{\gamma}$ is approximately determined by unit vector $e_i(\mathbf{x},\boldsymbol{\gamma})$, see (46). For the time dependence of the back–propagated scattered wavefield proportional to the local time dependence $f(\mathbf{x},t)$ of incident arrival (14), we define *imaging function*

$$\Phi(\mathbf{x},\boldsymbol{\gamma},\Delta t) = M\big(u_i(\mathbf{x},t'), e_i(\mathbf{x},\boldsymbol{\gamma}) f(\mathbf{x},t+\Delta t)\big) \quad . \tag{47}$$

The Fourier transform of the imaging function reads

$$\widehat{\Phi}(\mathbf{x},\boldsymbol{\gamma},\omega) = \widehat{\delta}(\omega) \int \mathrm{d}\Delta t \; \Phi(\mathbf{x},\boldsymbol{\gamma},\Delta t) \exp(\mathrm{i}\omega\Delta t) \quad . \tag{48}$$

The local time dependence $f(\mathbf{x},t)$ of the incident arrival is related to the local spectrum $\widehat{f}(\mathbf{x},\omega)$ through the inverse Fourier transform

$$f(\mathbf{x},t+\Delta t) = \frac{1}{2\pi\,\widehat{\delta}(\omega')} \int \mathrm{d}\omega' \; \widehat{f}(\mathbf{x},\omega') \exp[-\mathrm{i}\omega'(t+\Delta t)] \quad . \tag{49}$$

We insert (47) with (49) into (48). Since we are assuming that the imaging functional (8) is linear with respect to the second argument, we obtain

$$\widehat{\Phi}(\mathbf{x},\boldsymbol{\gamma},\omega) = \frac{1}{2\pi} \int \mathrm{d}\Delta t \int \mathrm{d}\omega' \; M\big(u_i(\mathbf{x},t'), e_i(\mathbf{x},\boldsymbol{\gamma}) \exp(-\mathrm{i}\omega' t)\big) \; \widehat{f}(\mathbf{x},\omega') \; \exp[\mathrm{i}(\omega-\omega')\Delta t] \; . \tag{50}$$

We integrate over Δt:

$$\widehat{\Phi}(\mathbf{x},\boldsymbol{\gamma},\omega) = \int \mathrm{d}\omega' \; M\big(u_i(\mathbf{x},t'), e_i(\mathbf{x},\boldsymbol{\gamma}) \exp(-\mathrm{i}\omega' t)\big) \; \widehat{f}(\mathbf{x},\omega') \; \delta(\omega'-\omega) \quad . \tag{51}$$

We integrate over ω':

$$\widehat{\Phi}(\mathbf{x},\boldsymbol{\gamma},\omega) = M\big(u_i(\mathbf{x},t'), e_i(\mathbf{x},\boldsymbol{\gamma}) \exp(-\mathrm{i}\omega t)\big) \; \widehat{f}(\mathbf{x},\omega) \quad . \tag{52}$$

5.2. Migrated section in terms of the angle–dependent reflectivity function

We insert the back–propagated scattered wavefield (46) into imaging functional (8), consider relation (52), and obtain approximation

$$m^{\mathrm{ArrEW}}(\mathbf{x}) \approx \int \mathrm{d}\omega \; \frac{-(\mathrm{i}\omega)^3}{8\pi^3\,\widehat{\delta}(\omega)\,\widehat{\delta}(\mathbf{k})} \oint \mathrm{d}\Gamma \; A(\mathbf{x},\boldsymbol{\gamma}) \; \frac{\widehat{\Phi}(\mathbf{x},\boldsymbol{\gamma},\omega)}{[c(\mathbf{x},\boldsymbol{\gamma})]^3} \\ \times \widehat{r}\big(\omega[\mathbf{p}(\mathbf{x},\boldsymbol{\gamma})-\mathbf{P}(\mathbf{x})],\boldsymbol{\gamma}\big) \exp\big\{\mathrm{i}\omega\,[p_k(\mathbf{x},\boldsymbol{\gamma})-P_k(\mathbf{x})]\,x_k\big)\big\} \tag{53}$$

of the migrated section. In this approximation, the migrated section is determined by the aperture weighting function (34), by the Fourier transform of imaging function (47), and by the Fourier transform of the angle–dependent reflectivity function (38).

5.3. Migrated section in terms of the reflectivity function

For each $\mathbf{x}$, vectorial argument $\mathbf{k}$ of the Fourier transform $\widehat{r}(\mathbf{k},\boldsymbol{\gamma})$ of the angle–dependent reflectivity function in relation (53) is parametrized by three parameters $\boldsymbol{\gamma} = (\gamma_1, \gamma_2)$ and ω:

$$\mathbf{k}(\mathbf{x},\boldsymbol{\gamma},\omega) = \omega[\mathbf{p}(\mathbf{x},\boldsymbol{\gamma}) - \mathbf{P}(\mathbf{x})] \quad . \tag{54}$$

We shall refer to wavenumber vector (54) as the *scattering wavenumber vector*. It is often called briefly the "scattering wavenumber" (Hamran & Lecomte, 1993; Lecomte & Gelius, 1998; Lecomte, 1999), and sometimes also the "combined wavenumber vector" or the "resolution vector" (Gelius, 1995).

Mapping (54) of $\boldsymbol{\gamma}$ and ω onto $\mathbf{k}$ is not single–valued. On the other hand, mapping (54) is very likely single–valued for $\boldsymbol{\gamma} \in \Gamma$ within angular domains Γ typical for seismic reflection surveys. Especially if the angular difference between direction $\boldsymbol{\gamma}$ corresponding to the ray leading to the source and direction $\boldsymbol{\gamma}$ corresponding to the rays leading to the receivers does not exceed $\frac{2}{3}\pi$ radians. Hereinafter, we shall assume that mapping (54) is single–valued for $\boldsymbol{\gamma} \in \Gamma$.

In the vicinity of each point $\mathbf{x}$, we define the *local wavenumber–domain reflectivity function* by relation

$$\boxed{\widehat{s}\big(\mathbf{x}, \omega[\mathbf{p}(\mathbf{x},\boldsymbol{\gamma}) - \mathbf{P}(\mathbf{x})]\big) = \widehat{r}\big(\omega[\mathbf{p}(\mathbf{x},\boldsymbol{\gamma}) - \mathbf{P}(\mathbf{x})],\boldsymbol{\gamma}\big)} \tag{55}$$

for scattering wavenumber vectors $\mathbf{k} = \mathbf{k}(\mathbf{x},\boldsymbol{\gamma},\omega)$ parametrized by $\boldsymbol{\gamma}$ and ω. The local wavenumber–domain reflectivity function $\widehat{s}(\mathbf{x},\mathbf{k})$ is defined by (55) for all $\mathbf{k} = \mathbf{k}(\mathbf{x},\boldsymbol{\gamma},\omega)$ corresponding to $\boldsymbol{\gamma} \in \Gamma$. For other wavenumber vectors $\mathbf{k}$, it may be either defined by (55) or put equal to zero.

In definition (55), the strong dependence of $\widehat{r}(\mathbf{k},\boldsymbol{\gamma})$ on wavenumber vector $\mathbf{k}$ is essential.

The dependence of $\widehat{r}(\mathbf{k},\boldsymbol{\gamma})$ on $\boldsymbol{\gamma}$ is moderate. The angular dependence of $\delta\varrho E_m e_m$ in definition (38) corresponds to the cosine of the angle between the two vectors, and the angular dependence of $\delta c_{ijkl} E_i P_j e_k p_l$ in definition (38) very roughly corresponds to the product of two cosines which should not change more rapidly than $\cos^2$. For a sufficiently narrow aperture moderately changing over the target zone, argument $\boldsymbol{\gamma}$ of $\widehat{r}(\mathbf{k},\boldsymbol{\gamma})$ in definition (55) may even be approximated by its mean value $\overline{\boldsymbol{\gamma}}$ within the target zone. The local wavenumber–domain reflectivity function $\widehat{s}(\mathbf{x},\mathbf{k}) \approx \widehat{r}(\mathbf{k},\overline{\boldsymbol{\gamma}})$ then becomes independent of $\mathbf{x}$.

Even for a wide aperture, the dependence of $\widehat{s}(\mathbf{x},\mathbf{k})$ defined by (55) on $\mathbf{x}$ is moderate. For a sufficiently small target zone, position $\mathbf{x}$ in definition (55) may even be approximated by its mean value over the target zone, and the local wavenumber–domain reflectivity function $\widehat{s}(\mathbf{x},\mathbf{k}) \approx \widehat{s}(\overline{\mathbf{x}},\mathbf{k})$ becomes independent of $\mathbf{x}$.

Note that definition (55) may also be approximated by expression

$$\begin{aligned}\widehat{s}\big(\mathbf{x}, \omega[\mathbf{p}(\mathbf{x},\boldsymbol{\gamma}) - \mathbf{P}(\mathbf{x})]\big) \approx{}& \frac{\widehat{\delta\varrho}}{\varrho}\big(\omega[\mathbf{p}(\mathbf{x},\boldsymbol{\gamma}) - \mathbf{P}(\mathbf{x})]\big) E_m(\mathbf{x}) e_m(\mathbf{x},\boldsymbol{\gamma}) \\ &- \frac{\widehat{\delta c_{ijkl}}}{\varrho}\big(\omega[\mathbf{p}(\mathbf{x},\boldsymbol{\gamma}) - \mathbf{P}(\mathbf{x})]\big) P_i(\mathbf{x}) E_j(\mathbf{x}) p_k(\mathbf{x},\boldsymbol{\gamma}) e_l(\mathbf{x},\boldsymbol{\gamma}) \quad .\end{aligned} \tag{56}$$

This expression results from approximating $P_i(\mathbf{x}')$, $E_j(\mathbf{x}')$, $p_k(\mathbf{x}',\boldsymbol{\gamma}')$, $e_l(\mathbf{x}',\boldsymbol{\gamma}')$ in definition (38) by $P_i(\mathbf{x})$, $E_j(\mathbf{x})$, $p_k(\mathbf{x},\boldsymbol{\gamma}')$, $e_l(\mathbf{x},\boldsymbol{\gamma}')$ and inserting the approximation into definition (55).

We are now going to switch, in approximation (53) of the migrated section, from integration over $\boldsymbol{\gamma}$ and ω to integration over wavenumbers $\mathbf{k}$. The Jacobian of transformation (54) from $\boldsymbol{\gamma}$ and ω to $\mathbf{k}(\mathbf{x},\boldsymbol{\gamma},\omega)$ is

$$\frac{\mathrm{d}\mathbf{k}}{\mathrm{d}\Gamma \mathrm{d}\omega} = \frac{\omega^2}{[c(\mathbf{x},\boldsymbol{\gamma})]^3} |v_i(\mathbf{x},\boldsymbol{\gamma})[p_i(\mathbf{x},\boldsymbol{\gamma}) - P_i(\mathbf{x})]| \quad . \tag{57}$$

In approximation (53) of the migrated section, the local wavenumber–domain reflectivity function (55) is filtered with the local wavenumber resolution filter defined by relation

$$\widehat{w}\big(\mathbf{x}, \omega[\mathbf{p}(\mathbf{x},\boldsymbol{\gamma}) - \mathbf{P}(\mathbf{x})]\big) = -\frac{A(\mathbf{x},\boldsymbol{\gamma})}{|v_i(\mathbf{x},\boldsymbol{\gamma})[p_i(\mathbf{x},\boldsymbol{\gamma}) - P_i(\mathbf{x})]|} \frac{\widehat{\dot{\Phi}}(\mathbf{x},\boldsymbol{\gamma},\omega)}{\widehat{\delta}(\omega)} \, \widehat{\delta}(\mathbf{k}) \tag{58}$$

for all scattering wavenumber vectors $\mathbf{k} = \omega[\mathbf{p}(\mathbf{x},\boldsymbol{\gamma}) - \mathbf{P}(\mathbf{x})]$ corresponding to $\boldsymbol{\gamma} \in \Gamma$, and equal to zero for other wavenumber vectors $\mathbf{k}$.

The local wavenumber resolution filter (58) is specified in terms of the aperture weighting function (34) and 1–D Fourier transform

$$\widehat{\dot{\Phi}}(\mathbf{x},\boldsymbol{\gamma},\omega) = -\mathrm{i}\omega \, \widehat{\Phi}(\mathbf{x},\boldsymbol{\gamma},\omega) \tag{59}$$

of the derivative $\dot{\Phi}(\mathbf{x},\boldsymbol{\gamma},\Delta t)$ of the imaging function.

In definition (58), the dependence of $\widehat{w}(\mathbf{x},\mathbf{k})$ along lines $\mathbf{k} = \omega[\mathbf{p}(\mathbf{x},\boldsymbol{\gamma}) - \mathbf{P}(\mathbf{x})]$ parametrized by ω is determined just by the dependence of $\widehat{\dot{\Phi}}(\mathbf{x},\boldsymbol{\gamma},\omega)$ on ω. This dependence together with the aperture specified by the dependence of the aperture weighting function $A(\mathbf{x},\boldsymbol{\gamma})$ on $\boldsymbol{\gamma}$ determine the essential properties of the local wavenumber resolution filter (58), which was already observed by Devaney & Oristaglio (1984), Wu & Toksöz (1987) or Dickens & Winbow (1991).

The dependence of $\widehat{\dot{\Phi}}$, p_k and v_l on $\boldsymbol{\gamma}$ is moderate. For a sufficiently narrow aperture, $\widehat{\dot{\Phi}}$, p_k and v_l on the right–hand side of definition (58) may even be approximated by their mean values with respect to $\boldsymbol{\gamma}$.

The dependence of A, $\widehat{\dot{\Phi}}$, P_k, p_k and v_l on $\mathbf{x}$ is also moderate. For a sufficiently small target zone, A, $\widehat{\dot{\Phi}}$, P_k, p_k and v_l on the right–hand side of definition (58) may even be approximated by their mean values with respect to $\mathbf{x}$, and the local wavenumber resolution filter $\widehat{w}(\mathbf{x},\mathbf{k}) \approx \widehat{w}(\overline{\mathbf{x}},\mathbf{k})$ becomes independent of position $\mathbf{x}$.

Approximation (53) of the migrated section then reads

$$\begin{aligned} m^{\mathrm{ArrEW}}(\mathbf{x}) \approx \int \mathrm{d}\omega \, \frac{\omega^2}{8\pi^3 \, \widehat{\delta}(\mathbf{k})} \oint \mathrm{d}\Gamma \, \frac{|v_i(\mathbf{x},\boldsymbol{\gamma})[p_i(\mathbf{x},\boldsymbol{\gamma}) - P_i(\mathbf{x})]|}{[c(\mathbf{x},\boldsymbol{\gamma})]^3 \, \widehat{\delta}(\mathbf{k})} \, \widehat{w}\big(\mathbf{x}, \omega[\mathbf{p}(\mathbf{x},\boldsymbol{\gamma}) - \mathbf{P}(\mathbf{x})]\big) \\ \times \widehat{s}\big(\mathbf{x}, \omega[\mathbf{p}(\mathbf{x},\boldsymbol{\gamma}) - \mathbf{P}(\mathbf{x})]\big) \exp\{\mathrm{i}\omega \, [p_k(\mathbf{x},\boldsymbol{\gamma}) - P_k(\mathbf{x})] \, x_k)\} \quad . \end{aligned} \tag{60}$$

We insert substitutions (54) and (57) into approximation (60). The migrated section then has the form of integral operator

$$m^{\mathrm{ArrEW}}(\mathbf{x}) \approx \frac{1}{8\pi^3 \, \widehat{\delta}(\mathbf{k})} \int \mathrm{d}\mathbf{k} \, \frac{\widehat{w}(\mathbf{x},\mathbf{k}) \, \widehat{s}(\mathbf{x},\mathbf{k})}{\widehat{\delta}(\mathbf{k})} \, \exp(\mathrm{i} \, k_k \, x_k) \quad . \tag{61}$$

The right–hand side of relation (61) locally has the character of the Fourier transform of convolution.

We define the inverse Fourier transform of wavenumber–domain function $\widehat{s}(\mathbf{x},\mathbf{k})$ by relation

$$s(\mathbf{x},\mathbf{x}')\frac{1}{8\pi^3\,\widehat{\delta}(\mathbf{k})}\int\mathrm{d}\mathbf{k}\;\widehat{s}(\mathbf{x},\mathbf{k})\;\exp(\mathrm{i}\,k_k\,x'_k) \quad . \tag{62}$$

We analogously define the *local resolution function* $w(\mathbf{x},\mathbf{x}')$ as the inverse Fourier transform of the local wavenumber resolution filter $\widehat{w}(\mathbf{x},\mathbf{k})$ analogous to (62), and express approximation (61) in the spatial domain:

$$m^{\mathrm{ArrEW}}(\mathbf{x}) \approx \int\mathrm{d}\mathbf{x}'\;w(\mathbf{x},\mathbf{x}-\mathbf{x}')\;s(\mathbf{x},\mathbf{x}') \quad . \tag{63}$$

The right–hand side of relation (63) locally has the character of convolution. Since the dependence of function $s(\mathbf{x},\mathbf{x}')$ on $\mathbf{x}$ is moderate, we may use approximation

$$s(\mathbf{x},\mathbf{x}') \approx s(\mathbf{x}',\mathbf{x}') \tag{64}$$

for all points $\mathbf{x}$ from the vicinity of point $\mathbf{x}'$. The dependence of $s(\mathbf{x},\mathbf{x}')$ on $\mathbf{x}$ becomes evident on a global rather than local scale. For each $\mathbf{x}$, the local resolution function $w(\mathbf{x},\mathbf{x}-\mathbf{x}')$ is concentrated in the vicinity of point $\mathbf{x}'=\mathbf{x}$. Because of this localization, we may insert approximation (64) into relation (63), and obtain expression

$$\boxed{m^{\mathrm{ArrEW}}(\mathbf{x}) \approx \int\mathrm{d}\mathbf{x}'\;w(\mathbf{x},\mathbf{x}-\mathbf{x}')\;r(\mathbf{x}')} \tag{65}$$

for the migrated section. Here

$$\boxed{r(\mathbf{x}') = s(\mathbf{x}',\mathbf{x}')} \tag{66}$$

is the *reflectivity function*.

In approximation (65), the dependence of the local resolution function $w(\mathbf{x},\mathbf{x}-\mathbf{x}')$ on coordinate difference $\mathbf{x}-\mathbf{x}'$ is essential, whereas its dependence on position $\mathbf{x}$ is moderate and becomes evident on a global rather than local scale.

For the figures of the local resolution functions in acoustic media refer to Hamran & Lecomte (1993), Lecomte & Gelius (1998), and Lecomte (1999).

5.4. Migrated section in terms of the reflection–transmission coefficient

We define locally, for points $\mathbf{x}'$ from the vicinity of point $\mathbf{x}$, the angle–dependent distribution

$$\boxed{R(\mathbf{x},\mathbf{x}',\boldsymbol{\gamma}) = \frac{r_{,k}(\mathbf{x}',\boldsymbol{\gamma})}{|v_i(\mathbf{x},\boldsymbol{\gamma})\,[p_i(\mathbf{x},\boldsymbol{\gamma})-P_i(\mathbf{x})]|}\;\frac{[p_k(\mathbf{x},\boldsymbol{\gamma})-P_k(\mathbf{x})]}{|\mathbf{p}(\mathbf{x},\boldsymbol{\gamma})-\mathbf{P}(\mathbf{x})|}} \tag{67}$$

of the weak–contrast displacement reflection–transmission coefficient. Partial derivatives $r_{,k}$ in (67) are related to variable $\mathbf{x}'$.

The Fourier transform of function (67), analogous to Fourier transform (43), reads

$$\widehat{R}(\mathbf{x},\mathbf{k},\boldsymbol{\gamma}) = \frac{\widehat{r}(\mathbf{k},\boldsymbol{\gamma})}{|v_i(\mathbf{x},\boldsymbol{\gamma})\,[p_i(\mathbf{x},\boldsymbol{\gamma})-P_i(\mathbf{x})]|}\;\mathrm{i}k_k\;\frac{[p_k(\mathbf{x},\boldsymbol{\gamma})-P_k(\mathbf{x})]}{|\mathbf{p}(\mathbf{x},\boldsymbol{\gamma})-\mathbf{P}(\mathbf{x})|} \quad . \tag{68}$$

Analogously to definition (55), we define for each point $\mathbf{x}$ the *local wavenumber distribution of the weak–contrast displacement reflection–transmission coefficient* by relation

$$\boxed{\widehat{S}\big(\mathbf{x},\omega[\mathbf{p}(\mathbf{x},\boldsymbol{\gamma})-\mathbf{P}(\mathbf{x})]\big) = \widehat{R}\big(\mathbf{x},\omega[\mathbf{p}(\mathbf{x},\boldsymbol{\gamma})-\mathbf{P}(\mathbf{x})],\boldsymbol{\gamma}\big) \quad .} \tag{69}$$

We insert (68) into (69) and obtain relation

$$\widehat{S}\big(\mathbf{x},\omega[\mathbf{p}(\mathbf{x},\boldsymbol{\gamma})-\mathbf{P}(\mathbf{x})]\big) = \widehat{r}\big(\omega[\mathbf{p}(\mathbf{x},\boldsymbol{\gamma})-\mathbf{P}(\mathbf{x})],\boldsymbol{\gamma}\big)\,\frac{\mathrm{i}\omega\,|\mathbf{p}(\mathbf{x},\boldsymbol{\gamma})-\mathbf{P}(\mathbf{x})|}{|v_i(\mathbf{x},\boldsymbol{\gamma})\,[p_i(\mathbf{x},\boldsymbol{\gamma})-P_i(\mathbf{x})]|} \quad . \tag{70}$$

The local wavenumber resolution filter analogous to filter (58), but corresponding to the local wavenumber distribution (70) of the weak–contrast displacement reflection–transmission coefficient, is defined by relation

$$\boxed{\widehat{W}\big(\mathbf{x},\omega[\mathbf{p}(\mathbf{x},\boldsymbol{\gamma})-\mathbf{P}(\mathbf{x})]\big) = \frac{A(\mathbf{x},\boldsymbol{\gamma})}{|\mathbf{p}(\mathbf{x},\boldsymbol{\gamma})-\mathbf{P}(\mathbf{x})|}\,\frac{\widehat{\Phi}(\mathbf{x},\boldsymbol{\gamma},\omega)}{\widehat{\delta}(\omega)}\,\widehat{\delta}(\mathbf{k})} \tag{71}$$

for scattering wavenumber vectors $\mathbf{k} = \omega[\mathbf{p}(\mathbf{x},\boldsymbol{\gamma})-\mathbf{P}(\mathbf{x})]$ corresponding to $\boldsymbol{\gamma} \in \Gamma$, and is equal to zero for other wavenumber vectors $\mathbf{k}$.

Analogously to relation (61), we approximate the migrated section by integral operator

$$m^{\mathrm{ArrEW}}(\mathbf{x}) \approx \frac{1}{8\pi^3\,\widehat{\delta}(\mathbf{k})}\int \mathrm{d}\mathbf{k}\;\frac{\widehat{W}(\mathbf{x},\mathbf{k})\;\widehat{S}(\mathbf{x},\mathbf{k})}{\widehat{\delta}(\mathbf{k})}\,\exp(\mathrm{i}\,k_k\,x_k) \quad . \tag{72}$$

The right–hand side of relation (72) has locally the character of the Fourier transform of convolution.

We define the inverse Fourier transform of wavenumber–domain functions $\widehat{W}(\mathbf{x},\mathbf{k})$ and $\widehat{S}(\mathbf{x},\mathbf{k})$ by relations analogous to (62), and express approximation (72) in the spatial domain:

$$m^{\mathrm{ArrEW}}(\mathbf{x}) \approx \int \mathrm{d}\mathbf{x}'\;W(\mathbf{x},\mathbf{x}-\mathbf{x}')\;S(\mathbf{x},\mathbf{x}') \quad . \tag{73}$$

The right–hand side of relation (73) has again locally the character of convolution. Since the dependence of function $S(\mathbf{x},\mathbf{x}')$ on $\mathbf{x}$ is moderate, we may use approximation

$$S(\mathbf{x},\mathbf{x}') \approx S(\mathbf{x}',\mathbf{x}') \tag{74}$$

for all points $\mathbf{x}$ from the vicinity of point $\mathbf{x}'$. The dependence of $S(\mathbf{x},\mathbf{x}')$ on $\mathbf{x}$ becomes evident on a global rather than local scale. For each $\mathbf{x}$, the local resolution function $W(\mathbf{x},\mathbf{x}-\mathbf{x}')$ is concentrated in the vicinity of point $\mathbf{x}' = \mathbf{x}$. Because of this localization, we may insert approximation (74) into relation (73), and obtain expression

$$\boxed{m^{\mathrm{ArrEW}}(\mathbf{x}) \approx \int \mathrm{d}\mathbf{x}'\;W(\mathbf{x},\mathbf{x}-\mathbf{x}')\;R(\mathbf{x}')} \tag{75}$$

for the migrated section. Here

$$\boxed{R(\mathbf{x}') = S(\mathbf{x}',\mathbf{x}')} \tag{76}$$

is the *spatial distribution of the weak–contrast displacement reflection–transmission coefficient.*

For example, in a case of a single planar interface $x_3 = x_3^0$ between two homogeneous media, the spatial distribution of the weak–contrast displacement reflection–transmission coefficient is $R(\mathbf{x}) = R\;\delta(x_3-x_3^0)$, where R is the plane–wave weak–contrast displacement reflection–transmission coefficient of Klimeš (2003, eq. 71). Within the Born approximation used throughout this paper, the plane–wave weak–contrast displacement reflection–transmission coefficient R is, naturally, the approximation of the

plane–wave displacement reflection–transmission coefficient (Červený & Ravindra, 1971) for very small contrasts of material parameters. For P–P scattering in isotropic media, the plane–wave weak–contrast displacement reflection–transmission coefficient R is equivalent to the reflection coefficient of Stolt & Benson (1986, eq. 1.7).

Approximation (75) has locally the character of convolution, because the dependence of the local resolution function $W(\mathbf{x}, \mathbf{x}-\mathbf{x}')$ on the coordinate difference $\mathbf{x}-\mathbf{x}'$ is essential, whereas the dependence of $W(\mathbf{x}, \mathbf{x}-\mathbf{x}')$ on position $\mathbf{x}$ is moderate and becomes evident on a global rather than local scale.

6. Numerical examples

The effect of convolution (65) on the structure in Figure 1 is demonstrated in Figures 2 and 3. We may assume, e.g., that the velocities are constant and that Figure 1 displays small density perturbations. Figures 2, 3 and 4 then show the images of the density which can ideally be obtained by prestack depth migration for a given configuration and source time function.

Acknowledgements

I am indebted to Paul Spudich who provided me with his perfect code I could modify to calculate the numerical examples presented here.

The research has been supported by the Grant Agency of the Czech Republic under contract P210/10/0736, by the Ministry of Education of the Czech Republic within research project MSM0021620860, and by the members of the consortium "Seismic Waves in Complex 3–D Structures" (see "http://sw3d.cz").

References

Červený, V. (2001): *Seismic Ray Theory.* Cambridge Univ. Press, Cambridge.

Červený, V. & Ravindra, R. (1971): *Theory of Seismic Head Waves.* Univ. Toronto Press, Toronto.

Claerbout, J.F. (1971): Toward a unified theory of reflector mapping. *Geophysics*, **36**, 467–481.

Devaney, A.J. & Oristaglio, M.L. (1984): Geophysical diffraction tomography. In: *Expanded Abstracts of 54th Annual Meeting (Atlanta)*, pp. 330-333, Soc. Explor. Geophysicists, Tulsa.

Dickens, T.A. & Winbow, G.A. (1991): Study of geophysical diffraction tomography. In: *Expanded Abstracts of 61nd Annual Meeting (Houston)*, pp. 963-966, Soc. Explor. Geophysicists, Tulsa.

Gelius, L.-J. (1995): Generalized acoustic diffraction tomography. *Geophys. Prospecting*, **43**, 3–29.

Hamran, S-E. & Lecomte, I. (1993): Local plane–wavenumber diffraction tomography in heterogeneous backgrounds. *J. seism. Explor.*, **2**, 133-146.

Klimeš, L. (2003): Weak–contrast reflection–transmission coefficients in a generally anisotropic background. *Geophysics*, **68**, 2063–2072, online at "http://sw3d.cz".

Lecomte, I. (1999): Local and controlled prestack depth migration in complex areas. *Geophys. Prospecting*, **47**, 799–818.

Lecomte, I. & Gelius, L.-J. (1998): Have a look at the resolution of prestack depth migration for any model, survey and wavefield. In: *Expanded Abstracts of 68th Annual Meeting (New Orleans)*, pp. 1112-1115, Soc. Explor. Geophysicists, Tulsa.

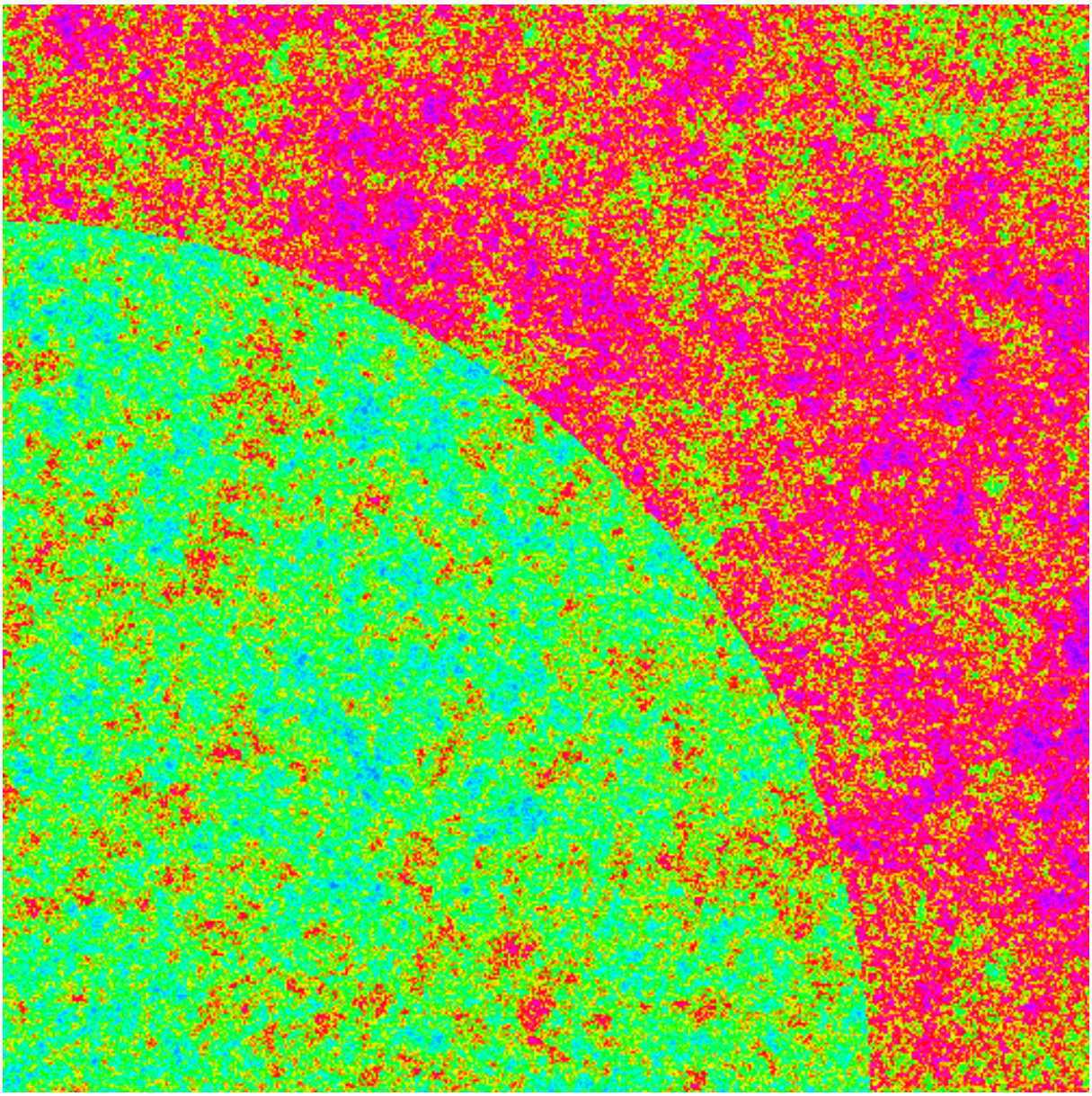

Figure 1. Structure of the target zone. A homogeneous quarter circle is superposed on a randomly generated representation of the self–affine medium in order to supplement random heterogeneities with a sharp interface. The target zone is assumed small compared with its depth below the source and receivers.

Stolt, R.H. & Benson, A.K. (1986): *Seismic Migration. Theory and Practice.* Handbook of Geophysical Exploration, Section I: Seismic Exploration, Vol. 5, Geophysical Press, London–Amsterdam.

Wu, R.-S. & Toksöz, M.N. (1987): Diffraction tomography and multisource holography applied to seismic imaging. *Geophysics*, **52**, 11–25.

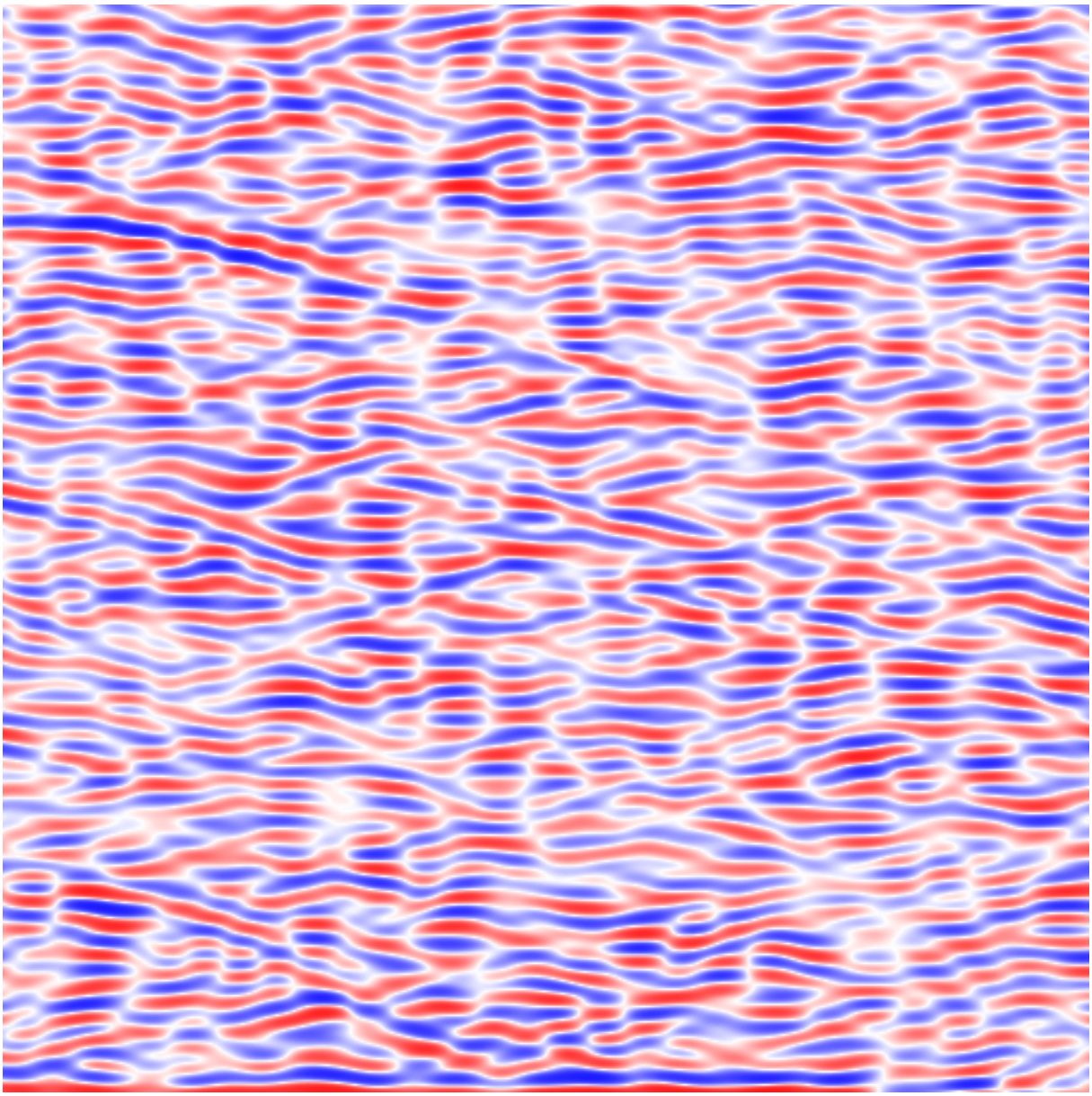

Figure 2. Common–shot prestack depth migrated section of the structure displayed in Figure 1, simulated according to equation (65) in a homogeneous velocity model. The imaging function is the Gabor signal with the predominant wavelength of 6% of the target zone dimension. The length of the symmetric receiver profile, with the source above the target zone (angle 0°), is twice the depth of the target zone, which corresponds to the aperture from −45° to 45°. Only wavenumber vectors between −22.5° and 22.5° are thus present in the image.

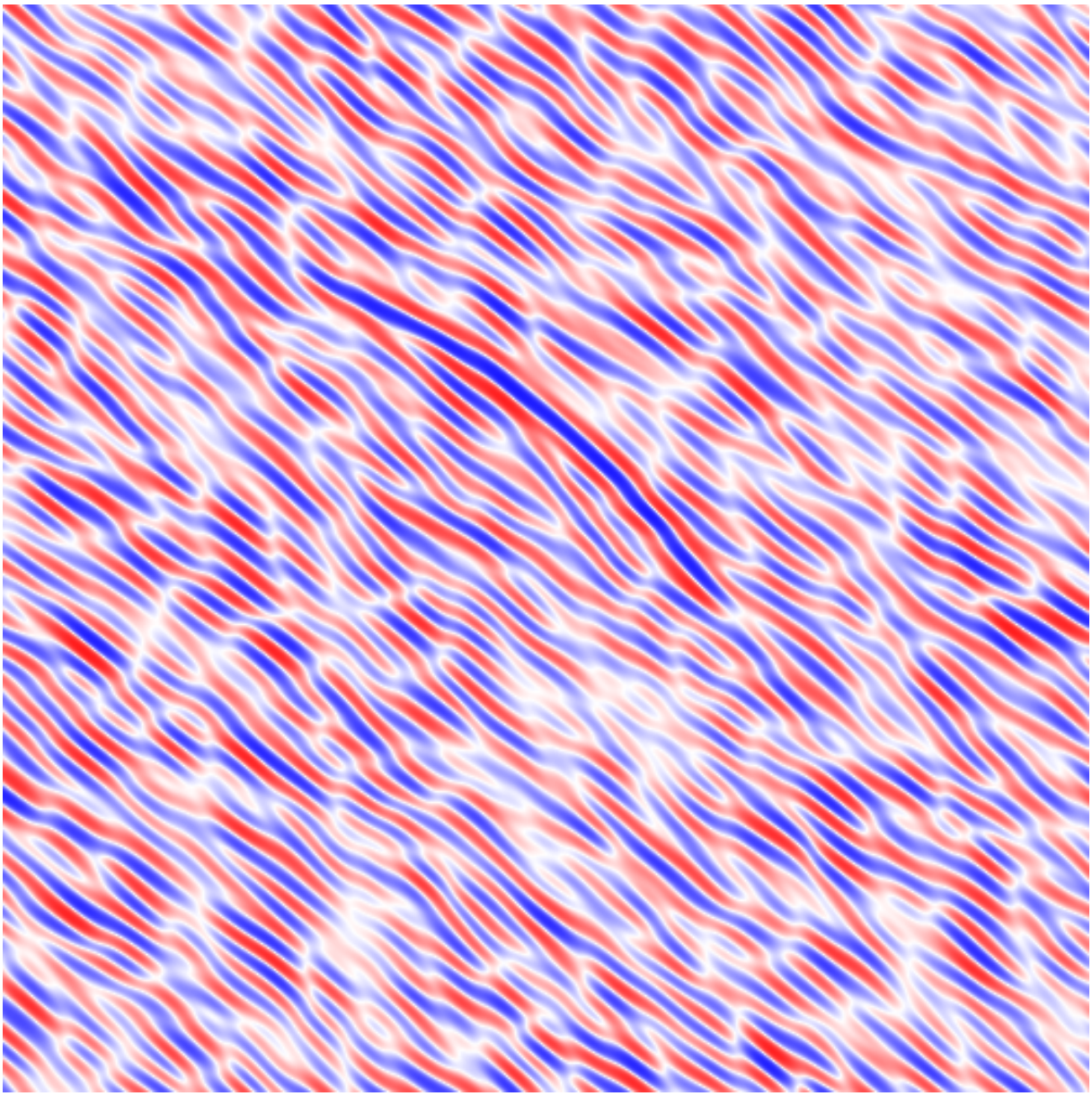

Figure 3. Common–shot prestack depth migrated section of the structure displayed in Figure 1, simulated according to equation (65) in a homogeneous velocity model. The symmetric receiver profile from Figure 2 has been shifted to the right, locating the leftmost receiver above the target zone. The source is thus in the direction of 45° and the aperture extends from 0° to 63°. Only wavenumber vectors between 22.5° and 54° are thus present in the image.

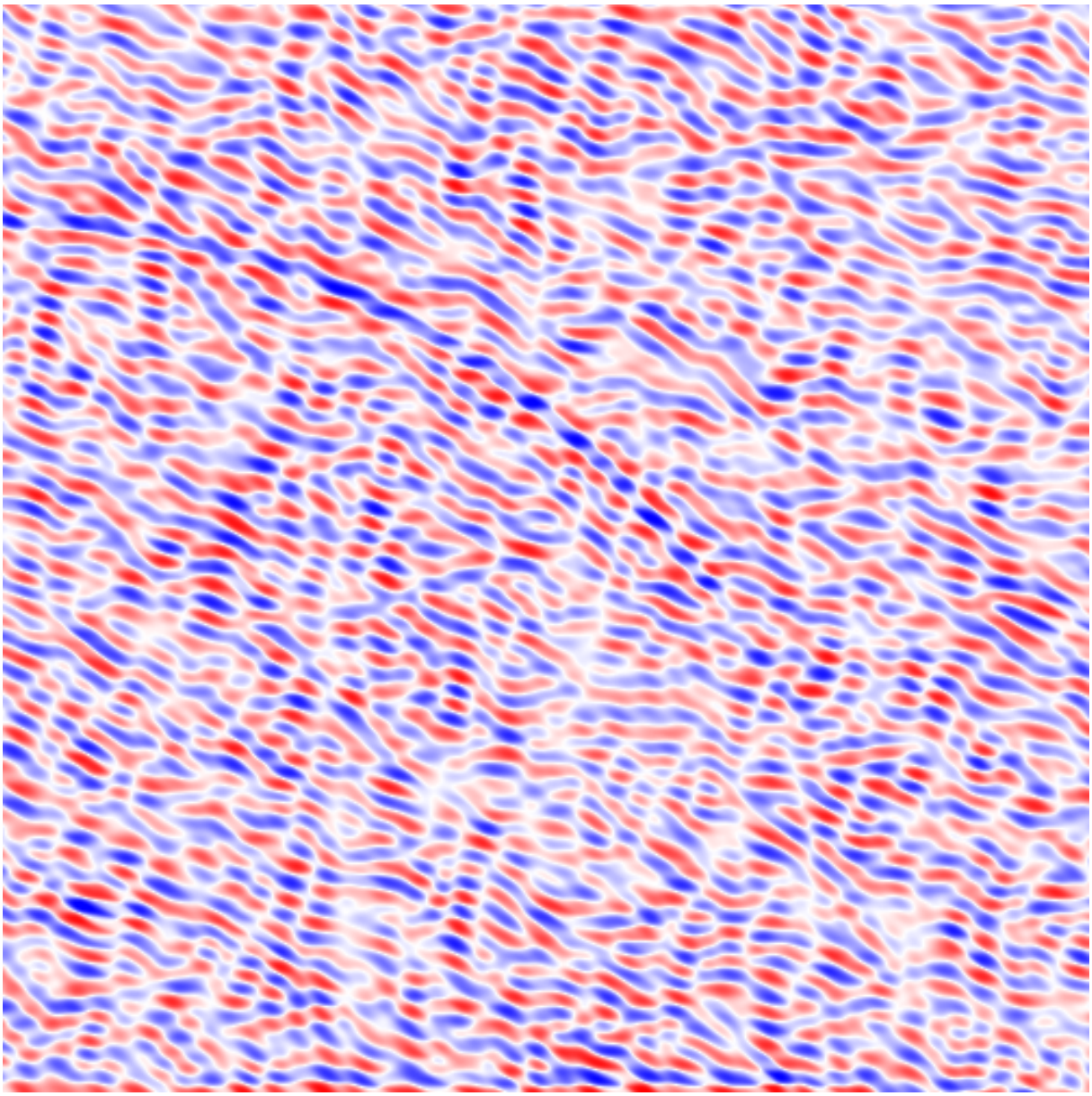

Figure 4. Sum of the common–shot prestack depth migrated sections of Figures 2 and 3. Let us emphasize that Figures 2, 3 and 4 are not the result of a particular migration: they show which features of the structure can be resolved by the ideal migration (no multiples, no noise, no transmission losses, perfect velocity model, exact calculation of elastic wavefields).